Combining gravitational and electromagnetic waves observations to investigate local structure and the Hubble tension

Brayan Yamid Del Valle Mazo[2,3], Antonio Enea
Romano[1,2,3], and Maryi Alejandra Carvajal Quintero[2,3]

[1]*Theoretical Physics Department, CERN,CH-1211 Geneva 23, Switzerland*

[2]*ICRANet, Piazza della Repubblica 10,I–65122 Pescara, Italy*

[3]*Instituto de Fisica,Universidad de Antioquia,A.A.1226, Medellin, Colombia*

(Dated: June 22, 2021)

Abstract

Recent estimations of the Hubble parameter H_0 based on gravitational waves (GW) observations can be used to shed some light on the discrepancy between the value of the Hubble parameter H_0^P obtained from large scale observations such as the Planck mission, and the small scale value H_0^R, obtained from low redshift supernovae (SNe).

In order to investigate the origin of this discrepancy we perform a combined analysis of the luminosity distance of SNe and GW sources, using different methods, finding that the impact of the GW data is very limited, due to the small number of data points, and their large errors. We analyze separately data from the Pantheon and the Union 2.1 catalogues, finding that a model with H_0^P and a small local void can fit the data as well as a homogeneous model with H_0^R, resolving the apparent H_0 tension. We find that there is a significant difference between the size and depth of the inhomogeneity obtained using the two datasets, which could be due to the different sky coverage of the two catalogues. For Pantheon we obtain evidence of a local inhomogeneity with a density contrast $\delta_v = -0.155 \pm 0.026$, extending up to a redshift of $z_v = 0.056 \pm 0.0002$, while for Union 2.1 we obtain $\delta_v = -0.461 \pm 0.032$ and $z_v = 0.081 \pm 0.008$. We also perform some analysis using redshift shell averaged data, and obtain approximately the same results, hinting to the fact that the effects of the monopole component of the local inhomogeneity are the dominant ones.

arXiv:1912.12465v4 [gr-qc] 20 Jun 2021

I. INTRODUCTION

Recent gravitational wave observations [1] have provided a new estimation of the Hubble constant H_0, and could be used to shed some light on the tension between the large scale estimations based on the cosmic microwave background (CMB) radiation [2], and the value obtained analyzing low redshift SNe [3]. The latter analysis is based on the assumption that the Universe is well described by a spatially homogeneous solution of the Einstein's equations, but only an unbiased analysis of observations can actually confirm this hypothesis. As an alternative to dark energy it was proposed the existence of a very large local void [4–6], but large void models were incompatible with other observations, such as CMB. It was then investigated the effect of inhomogeneities in presence of dark energy [7], showing how they could lead to a correction of the apparent value of the cosmological constant, or affect [8, 9] the Hubble diagram. Other studies estimate the variance of H_0 using different analytical and numerical methods [10–12], but they do not perform an actual analysis of the observational data, so are not directly comparable to our results. We fit data without any homogeneity assumption. Our analysis is partially confirming the existence of a local underdensity surrounding us in different directions [13, 14].

There have been different approaches to the explanation of the H_0 tension [15–17], and it has been recently [18] claimed that there is no evidence of a local inhomogeneity, but in that analysis a fixed value of the absolute magnitude M was used, ignoring how it should change if H_0 is different, and instead of fitting directly the apparent magnitude, the intercept a_b was used, whose mathematical definition relies implicitly on some homogeneity assumptions. Here we will not propose any modification of the standard cosmological model, but only perform an unbiased analysis of SNe and GW sources luminosity distance data, in search of a possible evidence of peculiar velocity fields normally ignored when assuming a Friedmann–Lemaître–Robertson–Walker (FLRW) metric.

While number count observations only allow to measure directly the baryonic matter distribution, other effects such as gravitational lensing, allow to measure the total matter density, including the dark matter component, since gravitationally baryonic and dark matter produce the same gravitational effects. One possibility to overcome the difficulty of deducing the total density field from number counts, due for example to selection effects, is to reconstruct the total matter density distribution from the effects it imprints on the luminosity distance of standard candles [14], and standard sirens [19]. At low redshift the main effects of inhomogeneities on

the luminosity distance of the sources of electromagnetic waves, such as standard candles, is the Doppler effect [8, 20] due to the peculiar velocities of the sources and the observer, and a similar theoretical result holds also for the luminosity distance of GW sources [21]. It is consequently possible to apply the same reconstruction methods derived for standard candles [8, 14] to standard sirens, and perform a combined analysis of the luminosity distance of the sources of both gravitational and electromagnetic waves. At low redshift and in the perturbative regime the monopole of the effects on the luminosity distance is proportional to the volume average of the density contrast [8], and for an underdensity it corresponds to an outwardly directed peculiar velocity field pointing towards the outer denser region, implying a local increase of the Hubble parameter, which could account for the apparent difference between its large and small scale estimation.

Motivated by this apparent discrepancy we adopt an unbiased approach, i.e. we do not assume homogeneity, and let the data reveal whether the local Universe is in fact homogeneous or not. We analyze the luminosity distance data of supernovae (SNe) Ia from different catalogues combined with the luminosity distance of 9 GW sources identified by the Laser Interferometer Gravitational-Wave Observatory (LIGO) [1], and use this combined set of data to reconstruct the peculiar velocity field of the sources. The redshift of GW events not having an electromagnetic transient counterpart was obtained [1] by the LIGO collaboration by applying Bayesian analysis to the combined dataset of GW events and galaxy catalogues along the line of sight of the event.

We perform a combined analysis of the luminosity distance of SNe and GW sources, and we obtain different results using different SNe catalogues. We check if the peculiar velocity redshift correction applied to the Pantheon data could explain this difference, since Union 2.1 data is not redshift corrected, but we find that non redshift corrected Pantheon data lead to the same results. We also perform some analyses using redshift shell averaged data, and obtain approximately the same results, hinting to the fact that the effects of the monopole component of the local inhomogeneity are the dominant ones. The implications of the existence of a local underdensity are profound, since not taking it into proper account can produce a mis-estimation of all background cosmological parameters obtained under the assumption of large scale homogeneity, and can explain for example the apparent discrepancy between different measurements of the Hubble constant [8].

II.   DATASETS

We analyze two different supernovae datasets, the Union 2.1 catalogue from the Supernova Cosmology Project (SCP) [22], and the Pantheon catalogue [23], while for GW sources we use data from the LIGO collaboration [1]. The two different supernovae datasets lead surprisingly to very different conclusions in regards to the presence of a local underdensity.

The formulae we use are including relativistic effects, as shown by comparison with exact numerical calculations in [8], but if the peculiar velocity redshift correction is computed using an inaccurate formula often used to infer peculiar velocity from observations [24], the entire dataset can be affected. We used the second dataset published by the Pantheon collaboration [25], which removed some errors in the redshift correction at redshifts higher than the catalog depth. As explained in [8], the 2M++ catalogue used to estimate the peculiar velocity redshift correction, is not deep enough to eliminate the effects of an inhomogeneity extending beyond its depth $z = 0.067$. Note that the redshift edge of the inhomogeneity we obtain in our analysis is in fact around the depth of 2M++. It should also be noted that the effects of the homogeneity extend slighly beyond the edge, as shown in one example in fig.(1).

Using eq.(12), taking $D_L(z) = D_L^{obs}(z)$ and $\overline{D}_L(z)$ as the luminosity distance of a ΛCDM model with the parameters estimated by the Planck mission, we can obtain for each object the radial component of its peculiar velocity in a system of coordinates centered at our position. This procedure does not require to assume any spherical symmetry, since the general formula depends on the radial component of the peculiar velocity, and it only assumes that the dominant effect of the inhomogeneity is the Doppler effect, which is well justified at low redshift [8, 20], $z < 0.7$. Even using a cutoff of $z_{sup} = 0.5$ we get the edge of the inhomogeneity to be $z_v < 0.09$, so the formula can be used safely in this range.

The radial velocity field is not necessarily spherically symmetric with respect to the observer position, since there can be anisotropies in the local structure, but here we will focus on the monopole component. There is evidence that local structure is not isotropic [26], implying that extending the analysis to higher multipoles could also be important, but as a first step towards investigating the effects of local structure imprinted on the luminosity distance we will focus on the monopole. This can be done following two different approaches: computing shell averages of redshift and velocity data before analyzing them, which are by construction isotropic, or analyzing data without any averaging, assuming a model which includes the radial dependence, but ignores the possible angular dependence. The averaging procedures consists in dividing

4

the datasets in spherical shells of constant width $\delta z = 0.004$, and averaging the data inside each shell using inverse-variance weighting. We analyze data following both methods, finding a small difference between the results, hinting to the fact that the effects of anisotropies are not strong. In the formulae defining the χ^2 in the following sections, the variables z_i and v_i will represent the single data point or the shell average, depending on the fit.

III.   FITTING THE APPARENT MAGNITUDE DATA

The observed quantity is the apparent magnitude m, and analyzing it directly is preferable for the Pantheon dataset, since m is the quantity found in the publicly available data, not D_L, which is a derived quantity, and is model dependent, in the sense that it depends implicitly on M, which is a parameter of the model. In fact, from the definition of distance modulus $\mu = m - M$, we get

$$D_L(z) \; = \; 10^{\frac{\mu}{5}+1} = 10^{\frac{m-M}{5}+1} \,, \tag{1}$$

showing that in order to get D_L^{obs} from m^{obs} an assumption for M has to be made. There are two main advantages in using m :

- It is not necessary to derive D_L from m and propagate the errors, as shown above.

- It is not necessary to use different datasets for different values of $\{H_0, M\}$, since these are just parameters of the model, while for D_L they have to be assumed in order to obtain D_L^{obs} from m^{obs}. This allows to plot and compare directly the results of the fits corresponding to different values of $\{H_0, M\}$.

Using m it is clear the distinction between observed data and parameters of the model, while using D_L the parameter M is affecting both the model and D_L^{obs}, making the analysis less transparent. Theoretical predictions are normally made in terms of $D_L(z)$, but observational data analysis in models with varying $\{H_0, M\}$ should be preferably performed in terms of m. I¡

The theoretical model for m^{th} is related to the theoretical luminosity distance D_L^{th} by

$$m^{th} = 5 \log D_L^{th} - 5 + M \,, \tag{2}$$

and we compute the monopole effects of an hypothetical local inhomogeneity on D_L using the fomula [8]

$$D_L^{th}(z) = \overline{D_L^{th}}(z) \left[1 + \frac{1}{3} f \overline{\delta^{th}}(z) \right] \,, \tag{3}$$

where $\bar{\delta}(z)$ is the volume averaged density contrast and $\overline{D_L^{th}}(z)$ is the background luminosity distance of a ΛCDM model.

The dependency of the models on different parameters is given explicitly in the following equations

$$D_L(\Omega_i, H_0, I_i) = \overline{D_L}(\Omega_i, H_0) \left[1 + \frac{1}{3}f\bar{\delta}(I_i)\right], \tag{4}$$

$$m(\Omega_i, H_0, M, I_i) = 5 \log D_L(\Omega_i, H_0, I_i) - 5 + M, \tag{5}$$

where I_i are the parameters modelling the inhomogeneity. A homogeneous model is a special case of the general model given above, with $I_i = 0$. We do not make any assumption about the homogeneity of the local Universe, we just analyze data including the effects of a possible inhomogeneity. If the Universe were homogeneous our analysis should confirm it.

Note that as shown in [8, 14], a local inhomogeneity should only change the luminosity distance locally, since far from the inhomogeneity the volume averaged density contrast of a finite size homogeneity tends to zero.

IV. MODELING THE LOCAL INHOMOGENEITY

We model the local underdensity with a density profile of the type

$$\delta^{th}(\chi) = \delta_v[1 - \theta(\chi - \chi_v)], \tag{6}$$

where χ_v is the comoving distance of the edge of the inhomogeneity, δ_v the density contrast inside the inhomogeneity, and $\theta(x)$ is the Heaviside function. The corresponding volume averaged density contrast is

$$\overline{\delta^{th}}(z) = \left\{ \begin{array}{ll} \delta_v & z < z_v \\ \delta_v \left[\frac{z_v(1+z_v)}{z(1+z)}\right]^3 & z > z_v \end{array} \right\}, \tag{7}$$

where δ_v is the density contrast inside the inhomogeneity and z_v is the inhomogeneity edge redshift. The derivation of this formula is given in the appendix C. Using eq.(13) we get the following formula for the radial velocity profile

$$\frac{v_r(z)}{c} = \frac{1}{3}f \left\{ \begin{array}{ll} \delta_v\,z & for\ z < z_v \\ d\,/z^2 & for\ z > z_v \end{array} \right., \tag{8}$$

where the matching condition at z_v implies $d = \delta_v z_v^3$. Note that in deriving the last equation we have neglected the factor $(1 + z_v)/(1 + z)$, which is a good approximation, as shown in

fig.(1). The above formula is in agreement with the general result obtained in [8], confirmed by exact numerical calculations, according to which for low redshift inhomogeneities the effects are suppressed at high redshift by the volume in the denominator of the volume average.

We fit the data with this model by minimizing with respect to the two parameters δ_v, z_v the following $\chi^2(\delta_v, z_v)$

$$\chi^2 = \sum_i \left[\frac{m_i - m^{th}(z_i)}{\sigma_{m_i}} \right]^2 . \tag{9}$$

The results of the fit using the covariance matrix are given in the appendix.

The difference between our analysis and the one reported in [18] is presumably due to the fact therein it was assumed a fixed value of the absolute magnitude M, ignoring how it should change if H_0 is different, and instead of fitting directly the apparent magnitude, the intercept a_b was used, whose mathematical definition relies implicitly on some homogeneity assumptions. The difference between our analysis and [18] cannot be attributed to a difference in the choice of radial coordinate, since the luminosity distance as function of the redshift is an observational quantity, and such it is invariant under any coordinate transformation.

The above model is based on the very accurate low redshift approximation derived in [8], and on the assumption of a constant step density contrast profile as given in eq.(6). Note that since $\overline{\delta}(z)$ is the volume average of the density contrast, outside the inhomogeneity it is inversely proportional to the volume, and since at low redshift $\chi \approx z/aH_0$, we get the above expression outside the inhomogeneity, which is proportional to the inverse cube of the redshift. The factor $(1 + z)$ comes from the scale factor in $\chi \approx z/aH_0$, and at low redshift can be safely neglected. As shown in [8], by explicit comparison with exact numerical results, these approximations are quite accurate at low redshift.

It is important to note that the gravitational effects of the inhomogeneity extend slightly beyond its edge, due to the inverse cube suppression.
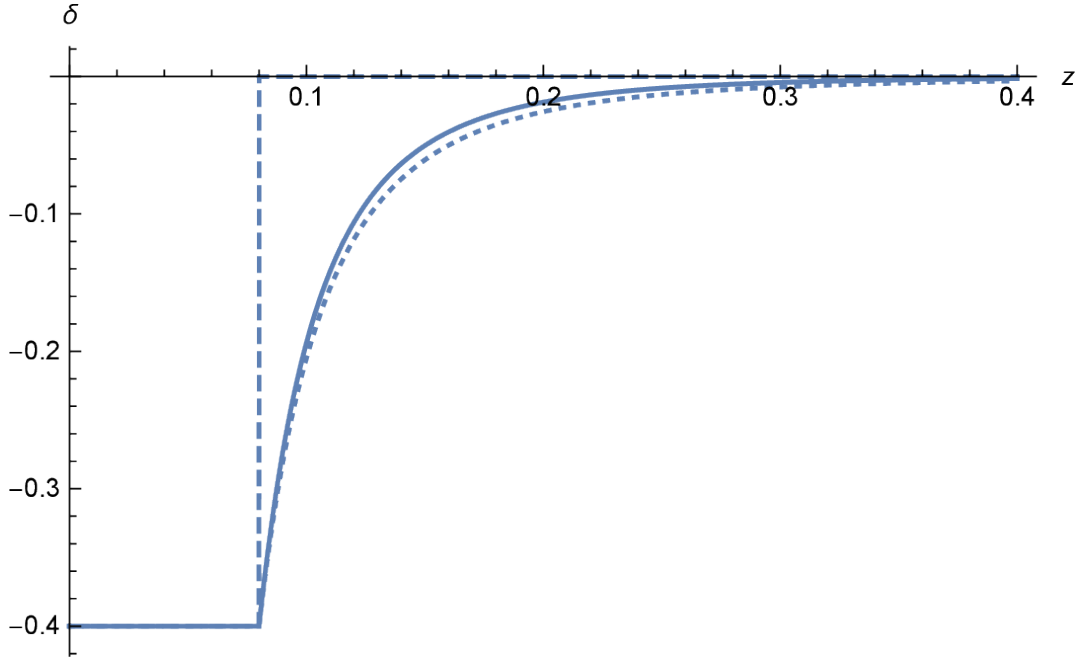
FIG. 1: The step density contrast δ (dashed) defined in eq.(6), its volume average $\bar{\delta}$ (solid) obtained in eq.(7), and the approximation (dotted) used to derive eq.(8) are plotted as a function of redshift for $z_v = 0.08$ and $\delta_v = -0.4$. The effects of the inhomogeneity are proportional to $\bar{\delta}$, and extend beyond the edge of the void, but are quickly suppressed beyond the edge, implying that high redshift observations are not affected by the local inhomogeneity.

V. FITTING CONSISTENTLY DATA WITH MODELS ASSUMING DIFFERENT VALUE OF H_0 AND M

Using only the definition of distance modulus and eq.(1) we derive in Appendix B a general model independent relation between different values of $\{H_0, M\}$ estimated at low redshift

$$M_a = M_b + 5 \log_{10} \left(\frac{H_a}{H_b} \right) , \tag{10}$$

which allows, for example, to obtain the implied Planck value of M^p from H_0^P and $\{H_0^R, M^R\}$, which are the values estimated in [3]. In the Appendix B we discuss the limits of validity of this relation, but when considering models with the same parameters Ω_i it can be safely applied, or more in general but at low red-shift, where $\{H_0, M\}$ are estimated. Note that a similar relation for M was used in [14] and more recently in [27]. There it was claimed it to be valid only for ΛCDM models, while our derivation is completely model independent. Using this relation, and assuming the values obtained in [3] as reference, we obtain M^P and fit m^{obs} with different

homogeneous and inhomogeneous models.

We denote with $m^{\mathrm{Hom}}(H_0^R)$ and $m^{\mathrm{Inh}}(H_0^P)$ respectively a homogeneous model with $\{H_0, M\} = \{H_0^R, M^R\}$ and an inhomogeneous model with $\{H_0, M\} = \{H_0^P, M^P\}$. We consider flat cosmologies with a Ω_m value estimated from the Planck mission data [1].

We fit data across different redshift ranges, to verify the robustness of the results. The results are summarized in Table I, and shown in fig.(2-3). As can be seen the χ^2 of $m^{\mathrm{Hom}}(H_0^R)$ is higher than that of $m^{\mathrm{Inh}}(H_0^P)$ for $z_{sup} = 0.11$, i.e. a model with H_0^P can fit better the low redshift SNe when the effects of a local small inhomogeneity are included in the analysis. For higher cutoffs the two models have approximately the same χ^2.

Note that the density contrast of the best fit underdensity is not large, and the hedge is located around the depth of the catalog $2M + +$ used in [3] for the redshift correction, supporting the argument [8] that the apparent tension between H_0^P and H_0^R is the consequence of a local inhomogeneity whose effects have not been removed by redshift correction, due to its size being comparable to the $2M++$ depth. As explained in [8] and evident from the plots, the local inhomogeneity does not affect the luminosity distance at high redshift, since the effect is proportional to the volume average of the density contrast, which tend to zero at high redshift, for a finite size inhomogeneity.

This kind of inhomogeneity could have been generated by a peak of primordial curvature perturbations [26], which is not a very unlikely event. Independently from the probability of being located inside of such an inhomogeneity, the unbiased data analysis we have performed is giving statistical evidence of its presence. This should be considered for its statistical significance more than for the theoretical estimation of its probability, i.e. the existence of inhomogeneities should be tested using observational data rather then being excluded a priori from the analysis, on the basis of theoretical predictions. Most of the GW sources are located outside this inhomogeneity, explaining why the H_0 value estimated from these objects is in agreement with the estimation based on other large scale observations such as the CMB.
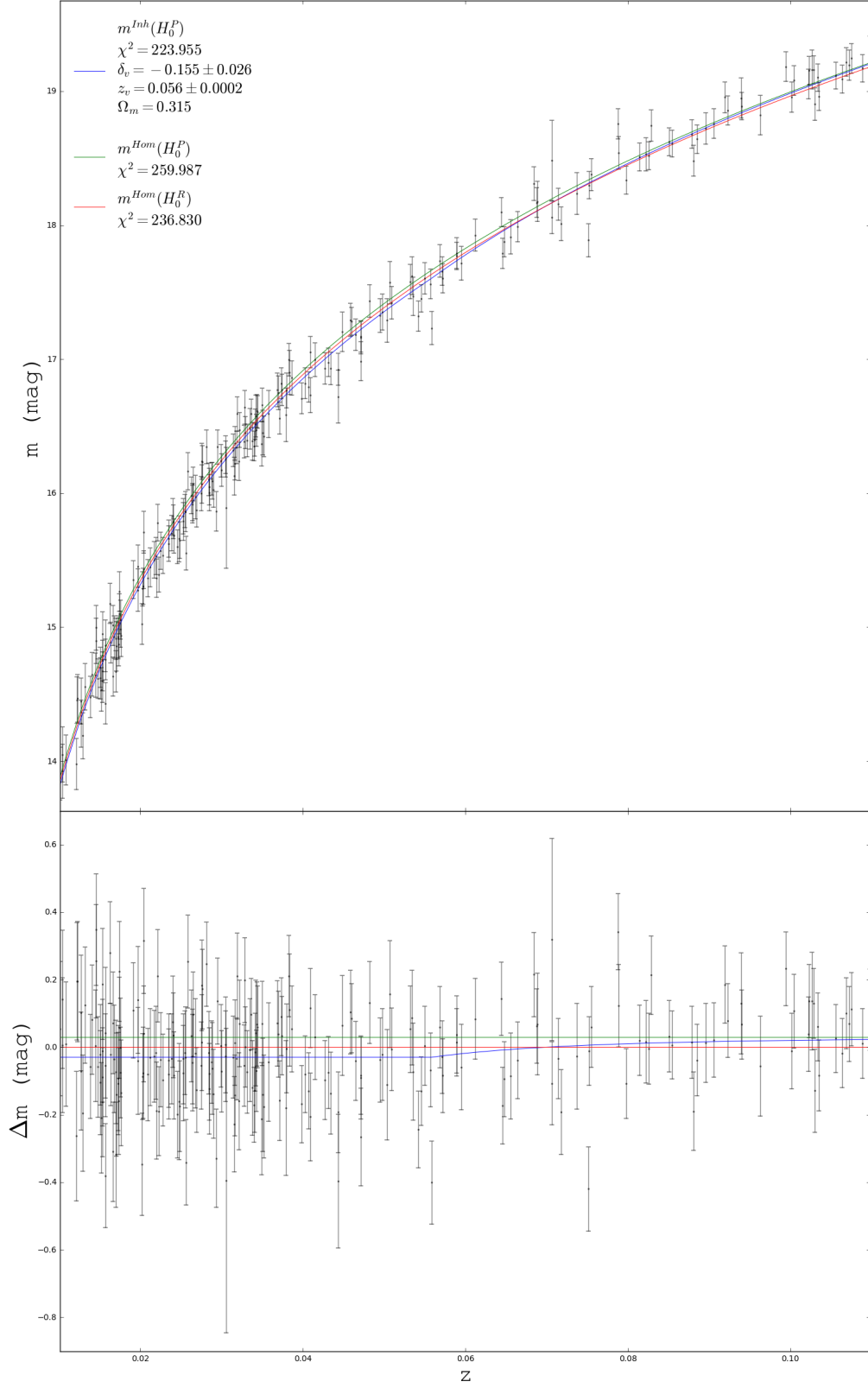
FIG. 2: Fit of Pantheon dataset with different models, for SNe with $z < 0.11$. In the lower panel is plotted for comparison purposes the difference between m and $m^{\mathrm{Hom}}(H_0^R)$, $\Delta m = m - m^{\mathrm{Hom}}(H_0^R)$. While $m^{\mathrm{Hom}}(H_0^P)$ does not provide a good fit of the data, $m^{\mathrm{Inh}}(H_0^P)$ is fitting the data better than $m^{\mathrm{Hom}}(H_0^R)$.
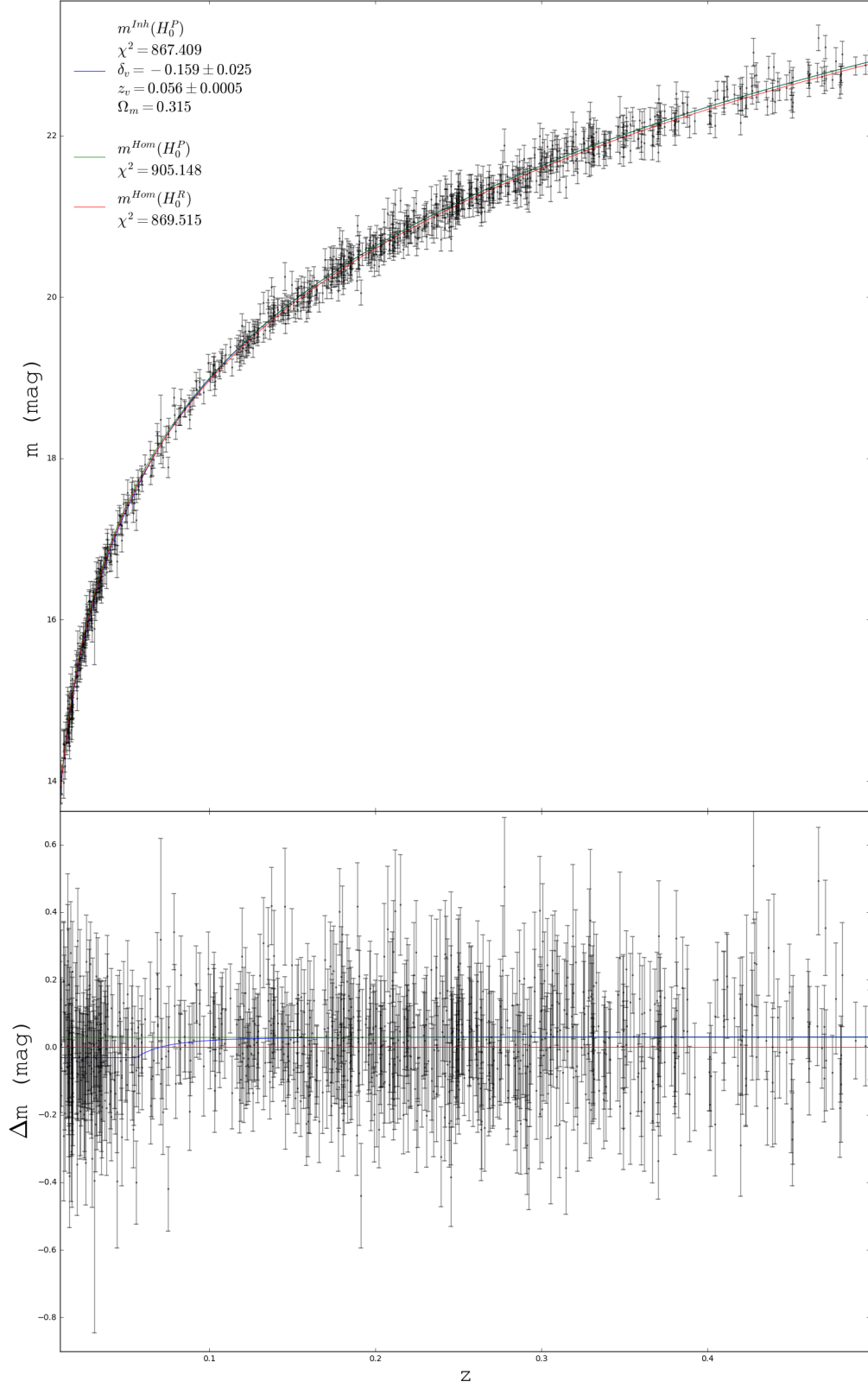
10

FIG. 3: Fit of Pantheon dataset with different models, for SNe with $z < 0.5$. In the lower panel is plotted for comparison purposes the difference between m and $m^{\mathrm{Hom}}(H_0^R)$, $\Delta m = m - m^{\mathrm{Hom}}(H_0^R)$. While $m^{\mathrm{Hom}}(H_0^P)$ does not provide a good fit of the data, the χ^2 of $m^{\mathrm{Inh}}(H_0^P)$ is approximately the same of $m^{\mathrm{Hom}}(H_0^R)$.

11

	$z_{sup} = 0.11$			$z_{sup} = 0.5$			$z_{sup} = 1.5$
	δ_v	z_v	χ^2	δ_v	z_v	χ^2	χ^2
$m^{\mathrm{Inh}}(H_0^P)$	-0.155 ± 0.026	$0.056 \pm 1.84 \times 10^{-4}$	223.955	-0.159 ± 0.025	$0.056 \pm 4.6 \times 10^{-4}$	867.409	1036.026
$m^{\mathrm{Hom}}(H_0^P)$	-	-	259.987	-	-	905.148	1073.773
$m^{\mathrm{Hom}}(H_0^R)$	-	-	236.830	-	-	869.515	1040.865

TABLE I: Results of the fits of the Pantheon data with different upper limits z_{sup} of the redshift range. An inhomogeneous model $m^{\mathrm{Inh}}(H_0^P)$ can fit the data better than a homogeneous model $m^{\mathrm{Hom}}(H_0^R)$ for $z_{sup} = 0.11$, while for higher cutoffs the χ^2 is approximately the same. This resolves the apparent H_0 tension, since at high redshift the local inhomogeneity does not affect the luminosity distance. The χ^2 for $z_{sup} = 1.5$ is obtained using the best fit parameters obtained for the $z_{sup} = 0.5$ fit.

VI. ANOTHER APPROACH TO THE RECONSTRUCTION OF THE PECULIAR VELOCITY FIELD FROM THE LUMINOSITY DISTANCE

Assuming the effects of the observer velocity have been removed, the dominant effect of inhomogeneities on the angular diameter distance at low redshift [28] is given by the radial component of the emitter peculiar velocity v_e

$$D_L(z) \approx \overline{D}_L(z) \left[1 + \frac{v_e \cdot \mathbf{n}}{z \, c} \right] , \tag{11}$$

where c is the speed of light, the unit vector $\mathbf{n}$ is in the direction of propagation from the emitter to the observer, and $\overline{D}_L(z)$ is the background angular diameter distance. In the above equation we have assumed that the peculiar velocity of the observer is zero, which is consistent with analyzing data from which our peculiar velocity with respect to the cosmic microwave background (CMB) has been subtracted, as is the case for the SNe Ia datasets we consider.

The background angular diameter distance $\overline{D}_L(z)$ is predicted theoretically for each value of z using the background cosmological parameters measured by large scale observations of the Universe, in our case the CMB measurements of the Planck [2, 29] mission, while $D_L(z)$ is the observed distance. It is then immediate to determine the radial component v_r of the peculiar velocity from eq.(11)

$$v_r = -v_e \cdot \mathbf{n} = -z \, c \left(\frac{D_L}{\overline{D}_L} - 1 \right) = -z \, c \delta D_L , \tag{12}$$

where we introduced the luminosity distance contrast δD_L, a dimensionless quantity which

accounts for the relative difference between the observed luminosity distance D_L and the corresponding background value $\bar{D}_L$. Note that the relation $v_r = -v_e \cdot \mathbf{n}$ is due the opposite direction of $\mathbf{n}$ with respect to the outwardly directed radial coordinate centered at the observer. Eq.(12) is the foundation of the reconstruction method we will apply, and allows to find the radial peculiar velocity field of the sources from the difference between their measured luminosity distance and the corresponding theoretical prediction obtained assuming a Friedman model with cosmological parameters obtained from independent large scale observations which are not sensitive to local inhomogeneities, such as the CMB [2, 8].

The monopole of the effects of local inhomogeneities can be computed by choosing a spherical coordinate system centered at the observer position, and after integrating the Euler's equations we get [30]

$$\frac{v_r(z)}{c} = -\frac{1}{3}f\bar{\delta}(z)z\,, \tag{13}$$

where $f = \frac{1}{H}\frac{\dot{D}}{D}$ is the growth factor and the volume averaged density contrast is defined as

$$\bar{\delta}(\chi) = \frac{3}{4\pi\chi^3}\int_0^\chi 4\pi\chi'^2\delta(\chi')\,d\chi'\,. \tag{14}$$

It has been shown in [8] (see fig.(2) and section 6 therein) that at low redshift the linear approximation adopted to obtain the above equations is in good agreement with exact numerical calculations in the redshift range of interest in this paper. Eq.(13) is the basis of our analysis since it allows to model appropriately the peculiar velocity field in terms of the density contrast. An underdensity induces an outwardly oriented velocity field, which if not distinguished from the large scale expansion due to the Hubble flow, can lead to an apparent discrepancy between the measurement of the Hubble constant obtained from local and large scale observations [8]. An inversion method to determine the density contrast from the luminosity distance contrast was derived in [8], but it involves derivatives with respect to the redshift, making it difficult to apply to observational data, while the peculiar velocity obtained using eq.(13) is more suitable for data analysis since it does not involve any derivative, and for this reason it is more convenient for data analysis purposes.

VII.   FITTING THE PECULIAR VELOCITY

In applying the reconstruction method we will assume the background cosmological parameters obtained by the Planck mission [1]. According to eq.(13) the radial velocity due to the monopole of the density contrast should be given by $v_r(z)/c = -\frac{1}{3} f \bar{\delta}(z) z$, which inside a region with constant density contrast δ_v gives $\bar{\delta}(z) = \delta_v$ and $v(z) \propto cz$. Motivated by the above considerations, we will fit the monopole of the low redshift peculiar velocity field inferred from luminosity distance observation assuming a linear relation of the form $v = m z + b$, and obtain the best fit parameters by minimizing the χ^2 defined as

$$\chi^2 = \sum_{i=1}^{N} \left[\frac{v_i - (m z_i + b)}{\sqrt{\sigma_{v_i}^2 + \sigma_{z_i}^2}} \right]^2 . \tag{15}$$

The parameter m is related to the volume averaged density contrast $\bar{\delta}$ by the relation $\bar{\delta}(z) = -\frac{3m}{fc}$. The results for the Union data fits are shown in fig.(5) and fig.(4). For both the averaged and the not averaged data, there is a strong statistical evidence of the presence of a radial velocity field directed outwardly, which corresponds to a volume averaged density contrast of about $\delta_v = -0.4$. The difference between the two fits, one with shell averaged data and the other with single data points, is a hint to the importance of anisotropies in this redshift range, i.e. for $z_{sup} = 0.0685$, but since this difference is not so large, it implies the monopole is producing the dominant effect.
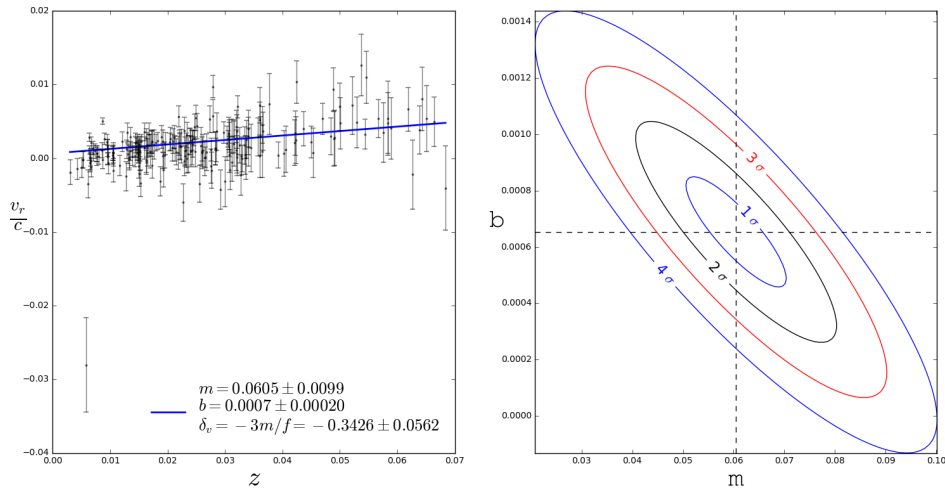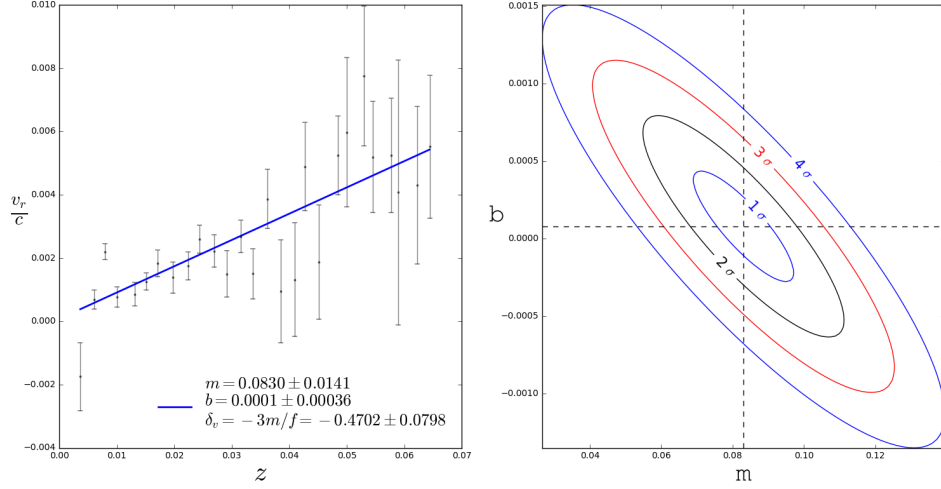

FIG. 4: Results of the fit of eq.(15) with not shell averaged data for the Union 2.1 data, and maximum redshift $z_{sup} = 0.0685$. We can exclude the $m = 0$ null hypothesis at more than 4σ confidence level.

FIG. 5: Results of the fit of eq.(15) with shell averaged data for the Union 2.1 data, and maximum redshift $z_{sup} = 0.0685$. We can exclude the $m = 0$ null hypothesis at more than 4σ confidence level. The shells have width $\Delta z = 0.004$.

VIII.   DETERMINING THE SIZE OF THE INHOMOGENEITY

We have shown that low redshift observations support the existence of a local underdensity, but it is also important to determine its size.
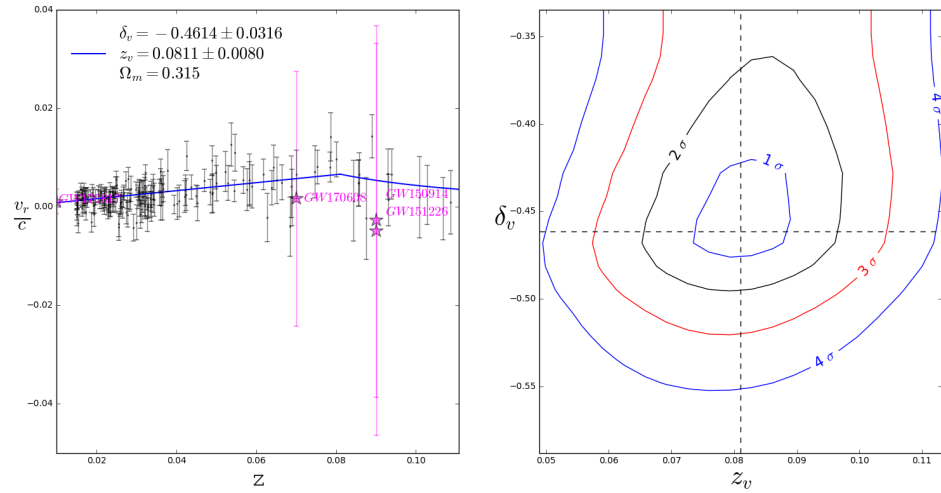

FIG. 6: Results of the fit of eq.(16) with not shell averaged data for the Union 2.1 data, and maximum redshift $z_{sup} = 0.11$. We can exclude the $\delta_v = z_v = 0$ null hypothesis at more than 4σ confidence level. The fitted data is a combination of the GW sources and SNe.
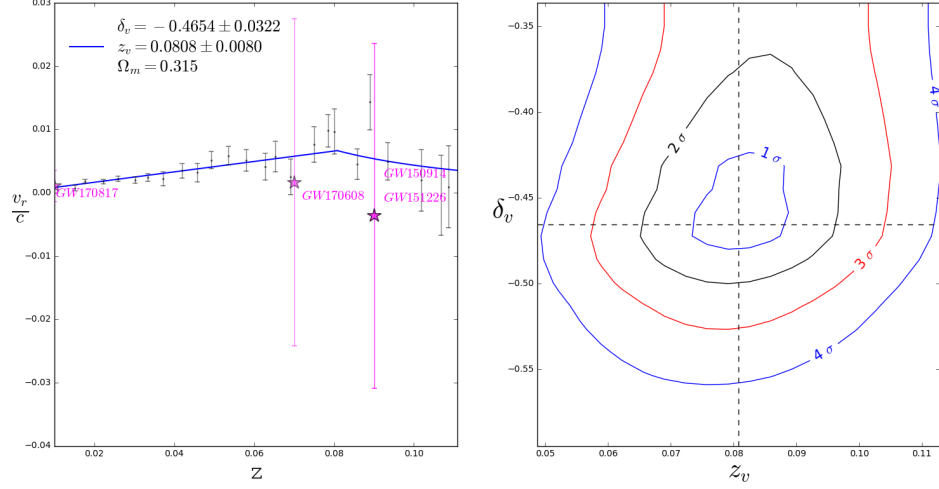
FIG. 7: Results of the fit of eq.(16) with shell averaged data for the Union 2.1 data, and maximum redshift $z_{sup} = 0.11$. We can exclude the $\delta_v = z_v = 0$ null hypothesis at more than 4σ confidence level. The shells have width $\Delta z = 0.004$, and the averages have been obtained by combining SN and GW sources data in the same shell. The fitted data is a combination of the GW sources and SNe.
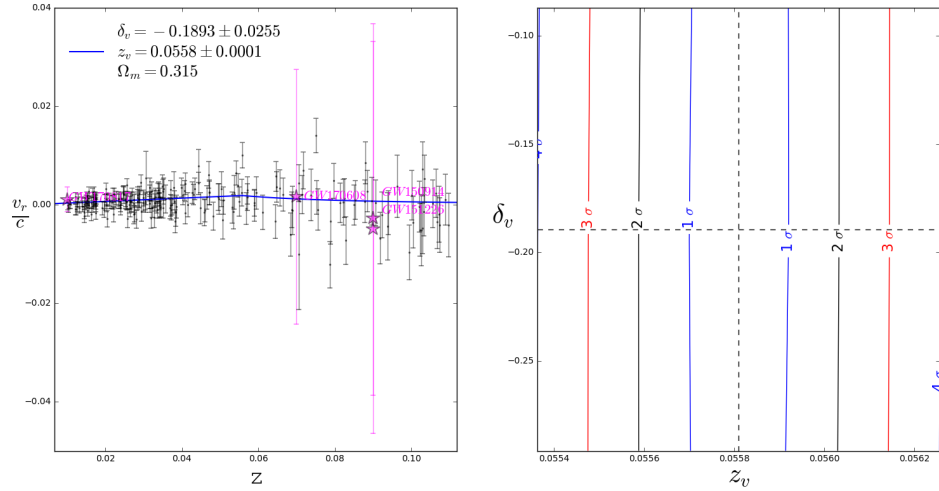

FIG. 8: Results of the fit of eq.(16) with not shell averaged data for the Pantheon data, and maximum redshift $z_{sup} = 0.11$. We can exclude the $\delta_v = z_v = 0$ null hypothesis at more than 4σ confidence level. The fitted data is a combination of the GW sources and SNe.
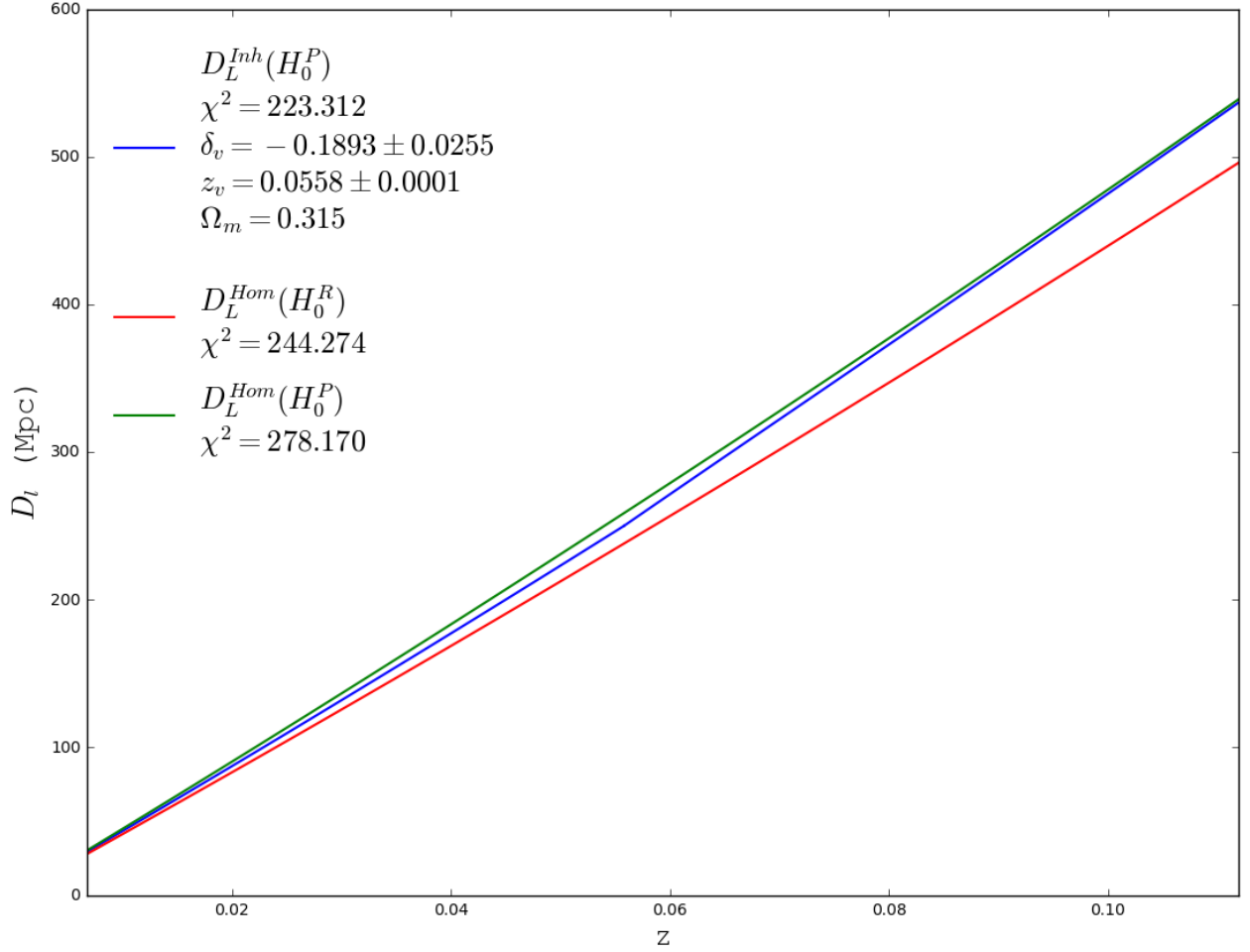
FIG. 9: Best fit inhomogeneous model $D_L^{\mathrm{Inh}}(H_0^P)$ obtained using the reconstruction method with the Pantheon data up to a redshift $z_{sup} = 0.11$. We also show the luminosity distance of the homogeneous models $D_L^{\mathrm{Hom}}(H_0^P)$ and $D_L^{\mathrm{Hom}}(H_0^R)$ for comparison purposes. The luminosity distance $D_L^{\mathrm{Inh}}(H_0^P)$ at high redshift tends as expected to $D_L^{\mathrm{Hom}}(H_0^P)$, implying that the inhomogeneity does not affect the large scale estimation of H_0, while at low redshift it is close to $D_L^{\mathrm{Hom}}(H_0^R)$.
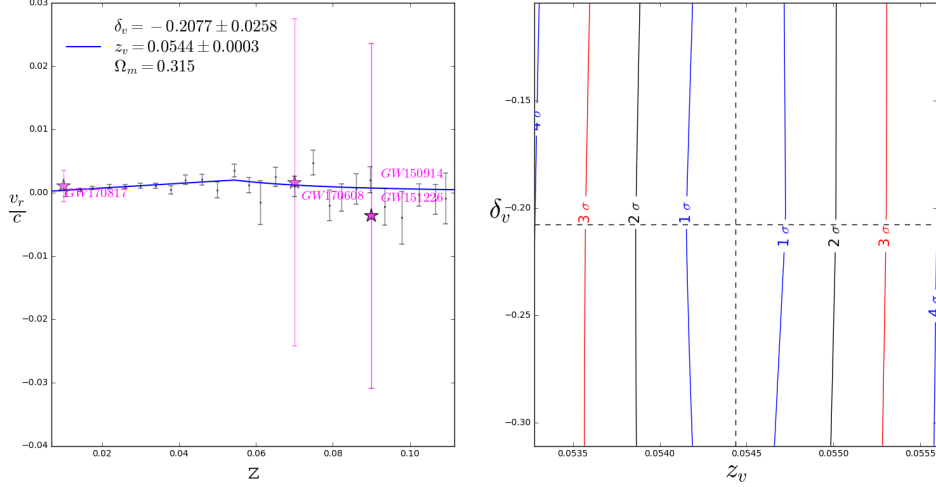
FIG. 10: Results of the fit of eq.(16) with shell averaged data for the Pantheon data, and maximum redshift $z_{sup} = 0.11$. The shells have width $\Delta z = 0.004$, and the averages have been obtained by combining SNe and GW sources data in the same shell. We can exclude the $\delta_v = z_v = 0$ null hypothesis at more than 4σ confidence level. The fitted data is a combination of the GW sources and SNe.

We fit the data with this model by minimizing with respect to the two parameters δ_v, z_v the following $\chi^2(\delta_v, z_v)$

$$\chi^2 = \sum_{z<z_v} \left(\frac{v_i - \frac{1}{3}f\delta_v z_i}{\sigma_{v_i}} \right)^2 + \sum_{z>z_v} \left(\frac{v_i - \frac{1}{3z_i^2}f\delta_v z_v^3}{\sigma_{v_i}} \right)^2 . \tag{16}$$

We perform two different fits, one without shell averaged data, and another with shell average, and the results are shown respectively in fig.(6) and fig.(7) for the Union 2.1 data and in fig.(8-9) and fig.(10) for the Pantheon data. As explained previously, depending on the type of fit the subindex i corresponds respectively to shell averages or to the single data points. As can be seen in the figures, the results of the fit using shell averaged data or single data points are very similar, hinting to the fact that the effects of anisotropies are not very strong.

The confidence contour plots show for both datasets the presence of a radial velocity field corresponding to a local underdensity, but the best fit parameters are quite different. This could be due to the different sky coverage of the two datasets, or the difference in the light curve fitting methods. The results of the Pantheon dataset are similar to the ones obtained fitting the apparent magnitude, showing that the inversion method is working well. Nevertheless the

18

direct fit of the apparent magnitude is preferable since it does not require to perform any error propagation for D_L, which can affect the accuracy of the inversion results.

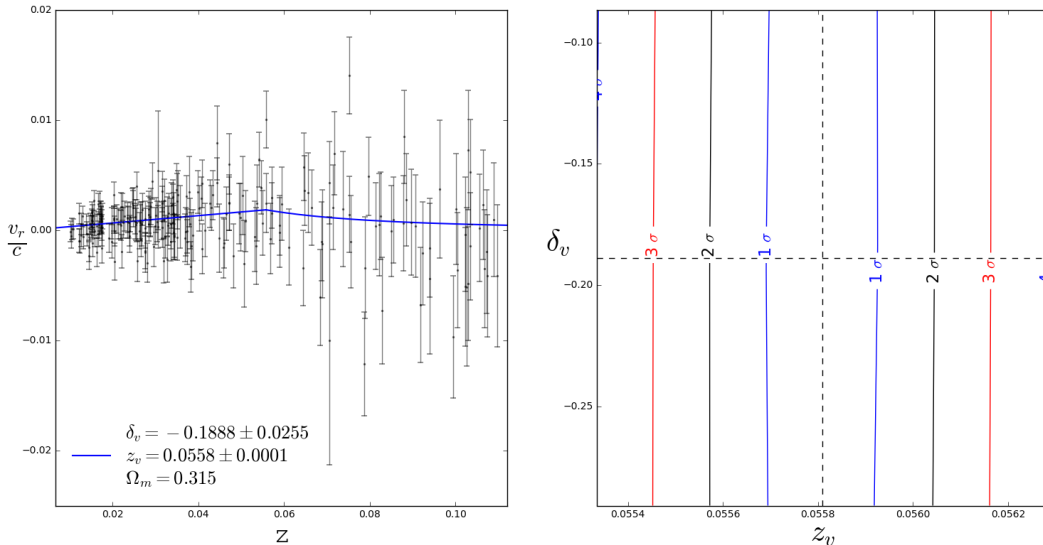## IX.   IMPACT OF THE GRAVITATIONAL WAVES DATA ON THE FIT RESULTS

FIG. 11: Results of the fit of eq.(16) with not shell averaged data for the Pantheon data, for a maximum redshift of $z_{sup} = 0.11$, and without including GW data. We can exclude the $\delta_v = z_v = 0$ null hypothesis at more than 4σ confidence level. The best fit value of the χ^2 is very close to the one obtained previously including GW data, implying that the latter is not very important, due to the limited number of data points, and large errors.

The peculiar velocity fits in the previous sessions were based on combining luminosity distance observations of GW sources and SNe. In this session we report the results of fitting only the SNe data, in order to assess the impact that these data have on the results. As shown in fig.(11), the impact of removing GW data on the parameters estimation is negligible. This can be explained by the limited number of data points and large errors, which limits the impact on the χ^2. When more GW data will be available we expect the impact to increase.

X.   CONCLUSIONS

We performed a combined analysis of the luminosity distance of SNe and GW sources, using different SNe catalogues. The results of our analysis show that the impact of the GW data is negligible, due to the limited number of data points and large errors. In our analysis we do include the effects of a possible local inhomogeneity, and make different assumptions for the value of H_0. We find that the data can be fitted equally well, and in some cases better, by a model with a small local inhomogeneity and the value of H_0 obtained by the Planck mission.

We have first fitted directly the apparent magnitude of SNe, and then introduced a method to reconstruct the peculiar velocity field from the luminosity distance, obtaining similar results with both methods. The results obtained for the direct fit of the apparent magnitude should nevertheless be preferred, since they do not require any error propagation associated to obtaining the luminosity distance from the apparent magnitude.

We found a significant difference between the size and depth of the inhomogeneity obtained analyzing the Pantheon data or the Union 2.1 data, which could be due to a difference in the sky coverage of the two datasets. The implications of the existence of this local underdensity could be profound, since not taking it into proper account can produce a mis-estimation of all background cosmological parameters obtained under the assumption of large scale homogeneity, and it can explain for example the apparent discrepancy between different measurements of the Hubble constant [8]. Most of the GW sources are located outside this inhomogeneity, and are not affected by it. This is in accord with the theoretical prediction of the effects of a local inhomogeneity, since the leading monopole perturbative effect is proportional to the volume averaged density contrast. The latter is inversely proportional to the cube of the distance from the point respect to which the monopole is computed, implying that the high redshift luminosity distance is not affected, including the distance of the last scattering surface from which the H_0 is estimated with CMB observations.

Our results are robust under different choices of the redshift range of the analyzed data, and the use of different methods to fit the data. The edge of the inhomogeneity is around the depth of the 2M++ catalogue used to compute the peculiar velocity redshift correction applied to the Pantheon data, which can naturally explain why such procedure did not remove the effects of the inhomogeneity obtained in our analysis.

In the future it will be important to confirm our results using other independent observables such as number counts[13], to include the effects of possible anisotropies, and investigate further

20

the cause of the difference between results obtained analyzing different SNe datasets.

Appendix A: Peculiar velocity redshift correction and SNe calibration

We can only measure the apparent magnitude of SNe, and in order to determine the corresponding luminosity distance, required to fit any cosmological model, a calibration is needed, since we do not have a direct measurement of the absolute luminosity. For low redshift SNe this is achieved by using the period-luminosity relation for Cepheids in the same galaxy of the SNe, which is calibrated using the NGC4258 megamaser angular diameter distance [31]. The measurement of the NGC4258 megamaser distance is of fundamental importance for the calibration of the Cepheid-SN Ia distance ladder. If the local Universe were not homogeneous the observed angular diameter distance would be affected, due to the gravitational effects which can be modeled quite precisely [8] using eq.(11), including that of NGC4258. The angular diameter distance is modified with respect to the background, due to the peculiar motion of the source with respect to the cosmic flow. The effects of peculiar velocities can be removed by applying a redshift correction (RC), which corresponds to eliminate the peculiar contribution from the observed redshift, to obtain a corrected redshift which should just be representative of the Hubble flow, and could be used for background cosmological parameters estimation.

Nevertheless, if the local inhomogeneity extends beyond the depth of the galaxy catalogue used to obtain the peculiar velocity field used for RC, its effects cannot be removed, and any background cosmological parameter obtained assuming homogeneity, because all inhomogeneities effects have supposedly been removed by RC, will be mis-estimated, including the Hubble parameter. A similar phenomenon can happen for the cosmological constant for example, leading to a correction of the parameters estimated assuming homogeneity [7], and a similar correction to the angular diameter distance of NGC4258 [31], or any other anchor used for calibration, could explain the discrepancy with the Planck estimation of H_0. Note that as explained in detail in [8], the effects of a local inhomogeneity on the high redshift luminosity distance are negligible, since the volume average of the density contrast tends to zero at infinity, making this effects only important for low redshift observations.

This correction can be well approximated as [8]

$$\frac{\Delta H^{app}(z)}{H_0^{true}} = -\frac{1}{3} f \bar{\delta}(z) \,, \tag{1}$$

where $\bar{\delta}$ is the volume average of the density contrast, and shows that an underdensity increases

the local apparent value with respect to the true background value. The implication of the above considerations is that when analyzing SNe data with models assuming different values of H_0, the absolute magnitude M has to be changed accordingly, as we will discuss in details in the next appendix.

Appendix B: The relation between H_0 and M

In order to clarify the relation between the observed quantity m^{obs}, and the parameters M and H, let's consider the relation between the distance modulus and the luminosity distance

$$\log_{10}(D_L) = 1 + \frac{\mu}{5}, \tag{1}$$

$$\mu = m - M, \tag{2}$$

and after defining $D_L = d/H_0$ we can obtain

$$m^{obs} = (5\log d - 5) + (M - 5\log H_0) = f(\Omega_i) + g(M, H_0) - 5, \tag{3}$$

$$f(\Omega_i) = 5\log d, \tag{4}$$

$$g(M, H_0) = M - 5\log H_0, \tag{5}$$

where the function f depends only on the cosmological parameters Ω_i. For example for a flat Universe we have

$$h(z) = \left[\Omega_m(1+z)^3 + \Omega_\lambda\right]^{1/2}, \tag{6}$$

$$d(z) = (1+z)\int^z \frac{dz'}{h(z')}, \tag{7}$$

$$D_L(z) = \frac{1}{H_0}d(z). \tag{8}$$

For other sets of cosmological parameters Ω_i numerical integration is required, but the general structure of eq.(5) would still be valid, i.e. it is always possible to write m^{obs} as the sum of two independent functions depending respectively on Ω_i and $\{H_0, M\}$. From eq.(5) it is evident that there is a degeneracy between the parameters H_0 and M, since keeping f constant, different combinations of $\{H_0, M\}$ can explain the same observational data m^{obs}, as long as $g = const$. In general the parameters $\{\Omega_i, H_0, M\}$ are independent, so the same observational data m^{obs} could be explained by different sets of values, and a joint analysis is required to obtain the best fit parameters. Nevertheless at low-redshift the function $f(\Omega_i)$ is only mildly dependent on Ω_i,

since at low-reshift we have that

$$D_L(z) = \frac{1}{H_0}\left(z + \frac{1-q_0}{2}z^2 + ..\right),$$ (9)

$$q_0 = \frac{3}{2}\Omega_m - 1,$$ (10)

so that at low redshift we have that $d \approx z$ is approximately independent of Ω_i, which is the Hubble law. This was indeed the reason for the need of high red-shift observations to obtain evidence of dark energy, since only higher order terms in the Taylor expansion of $D_L(z)$ depend on Ω_i, and also the reason why Einstein considered the cosmological constant its biggest mistake, since he did not know about the implications of the observation of higher redshift SNe.

Let's consider now the case of the two models for which the function d is the same, $d_a = d_b$, where we are denoting with subscripts a, b the values of the parameters for the two models. As explained above, at low redshit this should always be a good approximation, or it could be just an assumption, as for some of the fits we perform, with Ω_m fixed.

When the assumption that $d_a = d_b$ is justified according to the above arguments we get

$$g_a = g_b = M_a - 5\log_{10} H_a = M_b - 5\log_{10} H_b,$$ (11)

from which we finally obtain the following useful relations

$$D_L^a = D_L^b \frac{H_a}{H_b},$$ (12)

$$\mu_a = \mu_b + 5\log_{10}\left(\frac{H_b}{H_a}\right),$$ (13)

$$M_a = M_b + 5\log_{10}\left(\frac{H_a}{H_b}\right),$$ (14)

where the subscripts a and b correspond to different values of the parameters, i.e. $\{D_L^a, H_a, M_a\}$ and $\{D_L^b, H_b, M_b\}$. These formulae are related to the well known degeneracy [32] between H_0 and M. Note that a similar relation for M was derived in [27], but claimed to be valid only for ΛCDM models, while our derivation is completely model independent, and as explained above, we also observe that it is is valid only if $g_a = g_b$, which at high redshift cannot be assumed unless the Ω_i are fixed for different models. In any case even at high redshift the parameters Ω_i should not be too different among different models, so it can be considered approximately valid also at high redshift.

For the Pantheon dataset we have taken as reference the set of parameters $\{H_0 = 73.24 \pm 1.59, M = -19.25 \pm 0.71\}$ from [3], for Union 2.1 we use $M = -19.32$, and for Planck [2]

$H_0 = 67.4 \pm 0.5$. The values for the different parameters obtained using the formulae above are given in the Tables III and II.

Dataset	$H_0(km\,s^{-1}Mpc^{-1})$	M
Riess	73.24 ± 1.59	-19.25 ± 0.71
Planck	67.4 ± 0.5	-19.4 ± 0.65

TABLE II: Values of the parameters used in the analysis of the Pantheon data, obtained using the values in [3] as reference. The first row shows the values estimated by [3], and the second line the value of H_0 estimated by [2] and the corresponding value of M obtained from eq.(13). The underlined values are the publicly available ones and the not underlined are the values inferred using eq.(13).

Dataset	$H_0(km\,s^{-1}\,Mpc^{-1})$	M
Union 2.1	70	-19.32
Riess	73.24 ± 1.59	-19.2 ± 0.11
Planck	67.4 ± 0.5	-19.4 ± 0.04

TABLE III: Values of the parameters used in the analysis of the Union 2.1 data, obtained using the latter as reference. The underlined values are the publicly available ones and the not underlined are the values inferred using eq.(13).

When fitting data with models with different values of H_0 we changed the data according to the above equations. In the case of Pantheon the publicly available data gives m, from which μ is obtained using the corresponding M, while for Union 2.1 the distance modulus μ is given, which can be calibrated according to the above equations as well. For example, we can use the Pantheon dataset and fit the data assuming a value of H_0 equal to the Planck estimation, or use the Union data, and assume a value of H_0 equal to the one obtained in [3]. Note that this kind of calibration is not always correctly performed in the literature, leading to a an *implicit bias in the data analysis*. For example analyzing data allowing for a varying H_0, without consistently changing M is an inconsistent approach [18]. The above relations are based on the assumption that $d_a = d_b$, so they can be applied to homogeneous models using the same parameters Ω_i, or to the homogeneous regions of a locally inhomogeneous models, as long as in the homogeneous regions the condition $d_a = d_b$ is satisfied, as in the case of a locally inhomogeneous model we

consider. Inside the inhomogeneous region d can be different, even at low redshift and if the parameters Ω_i are the same, so a full fit of M could be required, but if most SNe are located outside the inhomogeneity, the formulae above should still give a good approximation.

It should be noted that the Pantheon dataset has been updated to correct an error in the calculation of the redshift correction [33, 34], which was applied to objects far beyond the depth of the galaxy catalogue used to obtain the peculiar velocities, and we use the second corrected version.

Appendix C: Derivation of the formula for $\bar{\delta}(z)$

In the case of a step density contrast profile of the type given in eq.(6), using the low redshift approximation $\chi \approx z/(aH_0) = z(1+z)/H_0$, the volume average of the density contrast outside the inhomogeneity at a comoving distance $\chi(z)$, can be computed as

$$\bar{\delta}(\chi) = \frac{3}{4\pi\chi^3} \int_0^\chi 4\pi\chi'^2 \delta(\chi')d\chi' = \frac{H_0^3}{[z(1+z)]^3}\delta_v\chi_v^3 = \delta_v \left[\frac{z_v(1+z_v)}{z(1+z)}\right]^3. \tag{1}$$

At low redshift, which is the regime of validity of the approximation, the factor $(1+z_v)/(1+z)$ can be safely neglected as shown in fig.(1).

Appendix D: Results of the fits of m using the covariance matrix

The results of the fit of the apparent magnitude using the covariance matrix to compute the χ^2 are given in the table below, showing that the results are approximately the same as the ones obtained ignoring the covariance, not affecting significantly the final conclusions.

	$z_{sup} = 0.11$			$z_{sup} = 0.5$			$z_{sup} = 1.5$
	δ_v	z_v	χ^2	δ_v	z_v	χ^2	χ^2
$m^{\mathrm{Inh}}(H_0^P)$	-0.142 ± 0.043	0.056 ± 0.0002	222.724	-0.173 ± 0.040	0.056 ± 0.0004	860.382	1031.940
$m^{\mathrm{Hom}}(H_0^P)$	-	-	233.139	-	-	878.889	1058.510
$m^{\mathrm{Hom}}(H_0^R)$	-	-	227.943	-	-	857.919	1027.149

TABLE IV: Results of the fit of the Pantheon data including the covariance matrix for m.

Appendix E: Fits of Pantheon data without peculiar velocity redshift correction

A peculiar velocity redshift correction is applied to the Pantheon data, consisting in subtracting the peculiar velocities inferred from the 2M++ galaxy catalog, while the Union 2.1 is not redshift corrected. In order to determine if this could be the cause of the difference in the results obtained for the two datasets, we remove the redshift correction using the publicly available data of the peculiar velocity [35].

The table below shows that the results for non redshift corrected data are approximately the same as those for redshift corrected data, excluding that redshift correction could be the cause of the above mentioned data fit results difference.

	$z_{sup} = 0.11$			$z_{sup} = 0.5$			$z_{sup} = 1.5$
	δ_v	z_v	χ^2	δ_v	z_v	χ^2	χ^2
$m^{\text{Inh}}(H_0^P)$	-0.156 ± 0.026	$0.056 \pm 1.5 \times 10^{-4}$	223.968	-0.159 ± 0.026	$0.056 \pm 8.22 \times 10^{-4}$	867.421	1036.039
$m^{\text{Hom}}(H_0^P)$	-	-	260.025	-	-	905.185	1073.810
$m^{\text{Hom}}(H_0^R)$	-	-	236.855	-	-	869.541	1040.891

TABLE V: Results of the analysis of the Pantheon data for non redshift corrected data.

Appendix F: Results of fits varying Ω_m

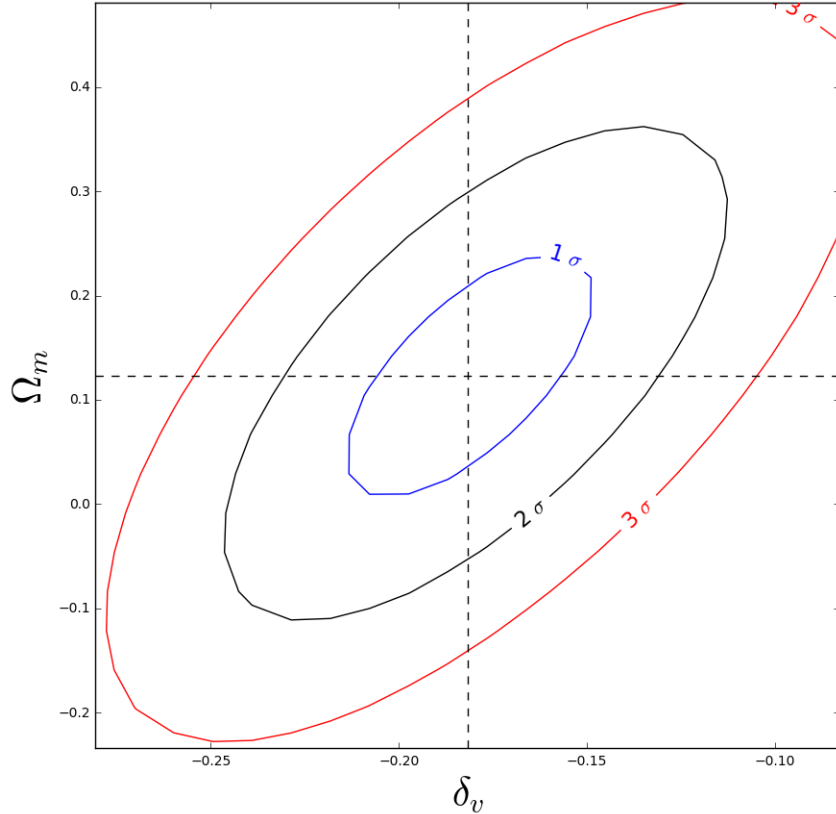We report below the results of the fit of the apparent magnitude varying also the parameter Ω_m.

FIG. 12: Contour plot of Ω_m and δ_v for the Pantheon dataset, corresponding to the model $m^{\text{Inh}}(H_0^P)$, with $z_{sup} = 0.11$.

	Ω_m	δ_v	z_v	χ^2
$m^{\text{Inh}}(H_0^P)$	0.123 ± 0.119	-0.182±0.033	0.065±0.001	222.694
$m^{\text{Hom}}(H_0^P)$	0.123	-	-	276.195
$m^{\text{Hom}}(H_0^R)$	$1.45 \times 10^{-5} \pm 0.944$	-	-	247.288

TABLE VI: Results of the fit of the apparent magnitude of the Pantheon dataset with $z_{sup} = 0.11$, without fixing the parameter Ω_m.

Comparing with Table I we can conclude that including Ω_m in the set of fitted parameters does not affect substantially the main results obtained fixing it, it just gives some slightly different estimation of the parameters of the inhomogeneity. Note that low redshift data is expected not to constrain strongly Ω_M, as we have obtained, since the main evidence of dark energy, and the consequent effect on the value of $\Omega_m = 1 - \Omega_\Lambda$, comes from high redshift SNe.

[1] LIGO Scientific, Virgo, B. P. Abbott *et al.*, (2019), arXiv:1908.06060.

[2] Planck, Y. Akrami *et al.*, (2018), arXiv:1807.06211.

[3] A. G. Riess *et al.*, Astrophys. J. **826**, 56 (2016), arXiv:1604.01424.

[4] M.-N. Celerier, Astron. Astrophys. **353**, 63 (2000), arXiv:astro-ph/9907206.

[5] K. Enqvist and T. Mattsson, JCAP **02**, 019 (2007), arXiv:astro-ph/0609120.

[6] J. Garcia-Bellido and T. Haugboelle, JCAP **04**, 003 (2008), arXiv:0802.1523.

[7] A. E. Romano and P. Chen, JCAP **10**, 016 (2011), arXiv:1104.0730.

[8] A. E. Romano, Int. J. Mod. Phys. **D27**, 1850102 (2018), arXiv:1609.04081.

[9] P. Fleury, C. Clarkson, and R. Maartens, JCAP **03**, 062 (2017), arXiv:1612.03726.

[10] I. Odderskov, S. Hannestad, and T. Haugbølle, JCAP **10**, 028 (2014), arXiv:1407.7364.

[11] I. Ben-Dayan, R. Durrer, G. Marozzi, and D. J. Schwarz, Phys. Rev. Lett. **112**, 221301 (2014), arXiv:1401.7973.

[12] V. Marra, L. Amendola, I. Sawicki, and W. Valkenburg, Phys. Rev. Lett. **110**, 241305 (2013), arXiv:1303.3121.

[13] R. C. Keenan, A. J. Barger, and L. L. Cowie, Astrophys. J. **775**, 62 (2013), arXiv:1304.2884.

[14] H. W. Chiang, A. E. Romano, F. Nugier, and P. Chen, JCAP **1911**, 016 (2019), arXiv:1706.09734.

[15] S. Vagnozzi, (2019), arXiv:1907.07569.

[16] E. Di Valentino, A. Melchiorri, O. Mena, and S. Vagnozzi, (2019), arXiv:1910.09853.

[17] SNLS, A. J. Conley *et al.*, Astrophys. J. Lett. **664**, L13 (2007), arXiv:0705.0367.

[18] W. D. Kenworthy, D. Scolnic, and A. Riess, Astrophys. J. **875**, 145 (2019), arXiv:1901.08681.

[19] LIGO Scientific, Virgo, 1M2H, Dark Energy Camera GW-E, DES, DLT40, Las Cumbres Observatory, VINROUGE, MASTER, B. P. Abbott *et al.*, Nature **551**, 85 (2017), arXiv:1710.05835.

[20] K. Bolejko *et al.*, Phys. Rev. Lett. **110**, 021302 (2013), arXiv:1209.3142.

[21] D. Bertacca, A. Raccanelli, N. Bartolo, and S. Matarrese, Phys. Dark Univ. **20**, 32 (2018), arXiv:1702.01750.

[22] R. Amanullah *et al.*, Astrophys. J. **716**, 712 (2010), arXiv:1004.1711.

[23] D. M. Scolnic *et al.*, The Astrophysical Journal **859**, 101 (2018).

[24] T. M. Davis and M. I. Scrimgeour, Mon. Not. Roy. Astron. Soc. **442**, 1117 (2014), arXiv:1405.0105.

[25] `https://github.com/dscolnic/Pantheon/blob/master/lcparam_full_long_zhel.txt`.

[26] A. E. Romano and S. A. Vallejo, EPL **109**, 39002 (2015), arXiv:1403.2034.

[27] G. Benevento, W. Hu, and M. Raveri, Phys. Rev. D **101**, 103517 (2020), arXiv:2002.11707.

[28] L. Hui and P. B. Greene, Phys. Rev. D **73**, 123526 (2006), arXiv:astro-ph/0512159.

[29] Planck, N. Aghanim *et al.*, Astron. Astrophys. **641**, A6 (2020), arXiv:1807.06209.

[30] P. J. E. Peebles, *Principles of physical cosmology* (Princeton University Press, 1993).

[31] M. Reid, D. Pesce, and A. Riess, Astrophys. J. Lett. **886**, L27 (2019), arXiv:1908.05625.

[32] D. Scolnic *et al.*, Astrophys. J. **859**, 101 (2018), arXiv:1710.00845.

[33] M. Rameez, (2019), arXiv:1905.00221.

[34] `https://github.com/dscolnic/Pantheon/issues/2`.

[35] `https://github.com/dscolnic/Pantheon/blob/master/sim_fitres/sim_combC110.FITRES`.